CHEMISTRY OF MATERIALS

pubs.acs.org/cm

Methods/Protocols

Quantification of Linker Defects in UiO-Type Metal−Organic Frameworks

Dag Kristian Sannes, Sigurd Øien-Ødegaard, Erlend Aunan, Ainara Nova, and Unni Olsbye*

Cite This: *Chem. Mater.* 2023, 35, 3793−3800

Read Online

ACCESS | Metrics & More | Article Recommendations | Supporting Information

ABSTRACT: Metal−organic frameworks (MOFs) are nanoporous materials composed of organic linkers and inorganic nodes. The large variety of linkers and nodes and the multiple ways to combine them make MOFs highly tunable materials, which are thoroughly studied for their use in, e.g., catalysis, gas capture, and separation. The chemistry of MOFs is further enriched by defects, e.g., missing linker defects, which provide active sites for catalysis or anchoring sites for introducing new functionalities. A commonly reported method to quantify linker defects assumes the presence of one type of linker and the complete removal of capping agents, solvents, and other impurities upon activation at high temperature, e.g., 400 °C (**M-400**). However, attempts to use this method for MOFs containing different types of linkers, also called multivariate MOFs (MTV-MOFs), or capping agents that are not completely removed at 400 °C, give inaccurate results and hamper comparing results from different publications. In this work, we have developed a new procedure to compute missing linker defects in Zr-based MOFs using standard analytical techniques to quantify the capping agents that remain in the MOF upon activation at 200 °C (**M-200**). This method, which has been tested in UiO-66/67 based MOFs, should be applicable to any MOF that (1) has known decomposition products, (2) has no missing cluster defects, (3) has empty pores or contain species that can be quantified after activation, and (4) has a known node composition at 200 °C.

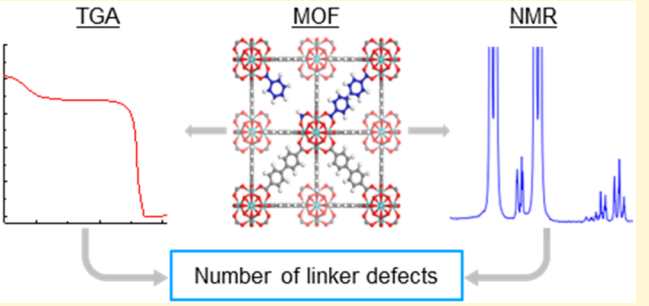

INTRODUCTION

MOFs are hybrid porous materials highly investigated for their use in many applications such as catalysis,[1,2] gas separation,[3,4] and electrochemistry.[5,6] MOFs are built from metal ions or clusters connected through multidentate organic linker molecules forming 2- or 3-dimensional structures. The synthesis of MOFs often requires the use of modulators to ensure reproducibility and achieve materials of high crystallinity. Modulators are commonly monocarboxylic acids (e.g., formic acid, acetic acid, and benzoic acid) or inorganic species (e.g., HCl).[7−10] These species reversibly bind to the metal cluster inhibiting the coordination of the linker—slowing down the crystal growth.[11,12] MOFs are highly tunable materials as both the node and the linkers can be replaced. As a result, over 90 000 MOF structures have been reported.[13]

Among the most studied MOFs for catalytic applications are UiO-66 and UiO-67[14] because of their high thermal,[15] mechanical,[16] and chemical stability.[17] The secondary building unit (SBU) of UiO-66/67 is the zirconium oxocluster, $Zr_6O_4(OH)_4^{12+}$, depicted in Figure 1. The zirconium cluster consists of six Zr atoms in an octahedral arrangement in which the eight facets are capped by alternating μ_3-O and μ_3-OH groups. Upon heating, the SBU undergoes a dehydration, effectively losing two water molecules. The coordination number and geometry of the zirconium changes from an 8-coordinated square antiprismatic to a distorted 7-coordinated monocapped trigonal prismatic,[18] while the coordination number for the SBU remains 12. For UiO-66 and UiO-67, each SBU is connected by 12 linker molecules, 1,4-benzenedicarboxylic acid and 4,4′-biphenyldicarboxylic acid, respectively. The high connectivity increases the stability of the material for two reasons. First, it gives rise to a highly rigid framework which has been shown to correlate with a stable framework.[19] Second, the high connectivity limits the accessibility to the Zr−O bond which inhibits hydrolysis.[20] The high stability of UiO type MOFs can also partly be attributed to the strong bond formed between Zr^{4+} and COO^-, which is due to strong coulombic forces between the carboxylate group and the high valent cation.[21]

Missing linker defects are formed from the incomplete ligand exchange reaction between the linker and modulator. The presence of defects is enhanced in UiO-66/67 because the strong interaction between Zr^{4+} and carboxylate slows down the rate of the ligand exchange reaction.[22] UiO-66/67 have

Received: December 19, 2022
Revised: April 22, 2023
Published: May 8, 2023

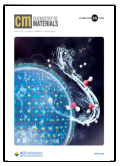

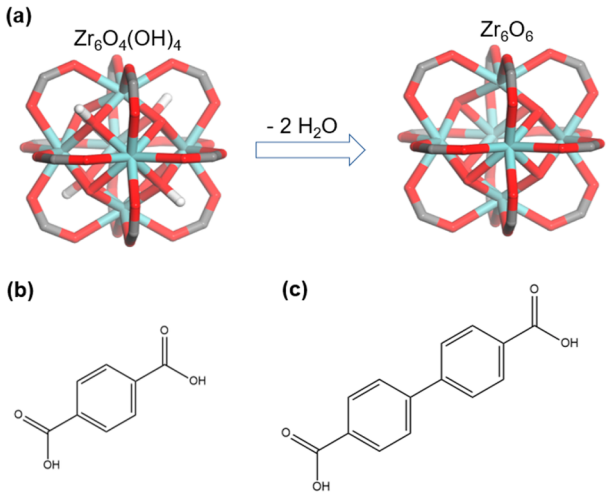

Figure 1. (a) Illustration of the hydrated and dehydrated zirconium cluster, charge compensated by carboxylate groups. (b) Illustration of the UiO-66 linker, 1,4-benzenedicarboxylic acid. (c) Illustration of the UiO-67 linker, 4,4′-biphenyldicarboxylic acid. Zirconium, oxygen, hydrogen, and carbon are shown in teal, red, white, and gray, respectively.

been heavily studied since their discovery in 2008,[23] and the first direct structural evidence of missing linker defects in UiO-66 was reported by Zhou et al. in 2013 using high resolution neutron powder diffraction.[24] Another important type of defects in UiO-66/67 is missing cluster defects (Figure 2), which were first thoroughly described by Goodwin et al. in 2014.[25] Recently this type of defect has received attention for increasing the accessibility of the metal nodes in the framework, thereby increasing the activity of the material.[26] Missing linker defects have been shown to be more prominent in samples synthesized at lower temperatures and with short crystallization periods.[10,26] Based on the work of Shearer et al., missing cluster defects are more prominent for samples synthesized using a high concentration of modulator with low pK_a values (especially for pK_a < 3.77) .[27]

Both missing linker and missing cluster defects can influence material properties such as surface area,[24] pore volume,[24] mechanical stability,[28] and thermal stability.[10] In addition, linker defects may change the number of active sites for catalysis or act as sites for further functionalization.[29] Thus, determining missing linker defects in an accurate and reproducible manner is extremely important to establish structure−property relationships and be able to compare results between different research groups. One of the most applied methods to quantify missing linker defects in UiO-66 was reported by Shearer et al. (See refs 14, 27, and refs therein). The major approximation in Shearer's method, labeled **M-400** in this work, is that all capping agents have been removed by 400 °C. The mass loss observed at temperatures higher than 400 °C, typically determined using Thermogravimetric Analysis (TGA) (see below), must then equal the mass loss of the linker molecules. The final MOF composition formula obtained by using this method is the following (eq 1):

$$Zr_6O_{4+2x+2y}(OH)_{4-2x-2y}(Linker)_{6-x}(capping\ agent)_{2y} \quad (1)$$

where the number of capping agents per Zr-node (2y) equals the number of open Zr sites, or linker defects, in the material after high-temperature treatment. The formula is derived in Supporting Information, Section 1.1.

A recently discovered weakness of this formula is that commonly used capping agents (i.e., functionalized linkers in MTV-MOFs and monocarboxylate species like benzoate) are only partially removed at 400 °C (Figure 3), causing a significant error in calculating the composition of the material. In these cases, when the formula is complemented by liquid phase nuclear magnetic resonance (NMR) spectroscopic measurements, the number of linkers and other capping agents may surpass the physically meaningful number (see Characterization and Discussion section, Table 1). Furthermore, the μ_3−O to μ_3−OH ratio must be changed to achieve charge balance, which is inconsistent with the 1 to 1 ratio expected at ambient conditions according to reported studies based on single crystal X-ray diffraction (XRD).[30,31]

As will be demonstrated below, those shortcomings can be eliminated if the molar mass of the MOF is determined after activation at 200 °C instead of 400 °C. In this work, this new strategy, labeled **M-200**, has been applied to seven UiO-66/67 samples, including MTV derivatives and temperature resistant modulators, but could easily be adapted for any MOF whose decomposition products and nodes composition at 200 °C are known (see Procedure section).

MATERIALS USED TO VALIDATE THE METHOD

A total of six UiO type MOFs have been synthesized to validate the **M-200** method for quantifying missing linker defects. A seventh sample was purchased commercially. The

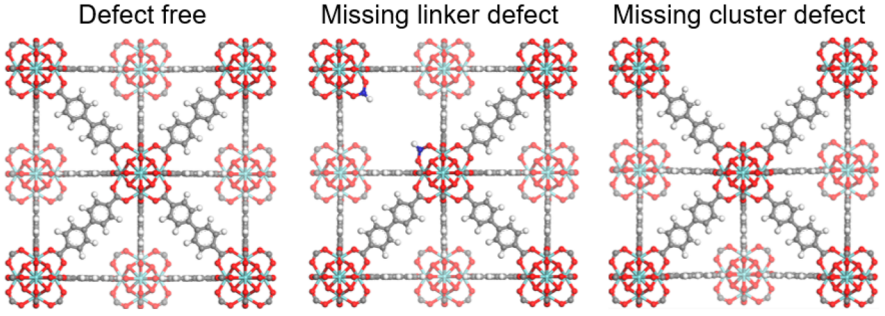

Figure 2. Illustration of the UiO-67 framework. Left: Ideal framework of UiO-67 in the absence of defects. Center: UiO-67 with two formate groups as capping agents. Right: UiO-67 with a missing cluster defect. Zirconium, oxygen, hydrogen, and carbon are shown in teal, red, white, and gray, respectively. Carbons in the monocarboxylates are shown in blue. Hydrogens coordinated to the nodes are omitted for clarity.

https://doi.org/10.1021/acs.chemmater.2c03744
Chem. Mater. 2023, 35, 3793−3800

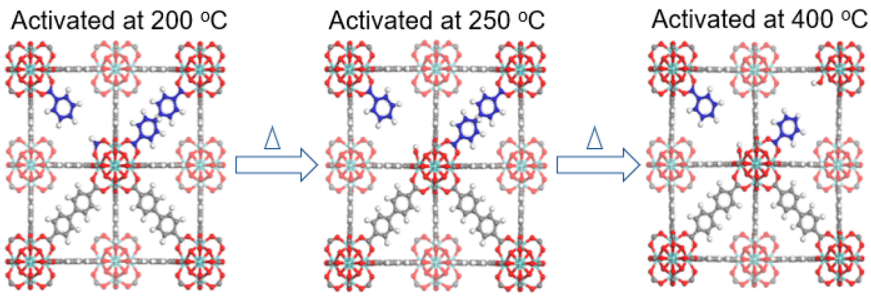

Figure 3. Left: Illustration of the UiO-67 framework after activation at 200 °C, with three benzoate capping agents and one formate capping agent. Middle: Illustration of the UiO-67 framework after activation at 250 °C, highlighting the low thermal stability of formate capping agents, which decomposes upon activation of the material above 200 °C. Right: Illustration of the UiO-67 framework after activation at 400 °C, highlighting the high thermal stability of benzoate capping agents which only partially decompose even after long exposure to high temperatures. Zirconium, oxygen, hydrogen, and carbon are shown in teal, red, white, and gray, respectively. Carbons in the monocarboxylates are shown in blue. Hydrogens coordinated to the nodes are omitted for clarity.

Table 1. Overview of the Calculated Chemical Formula of the UiO-66 and UiO-67 Samples Using Both the Old Method (M-400)[29] and the Method Presented in This Work (M-200)[a]

Sample	M-400	M-200
UiO-66-FA	$Zr_6O_{3.89}(OH)_{4.11}(BDC)_{5.81}(FE)_{0.49}$	$Zr_6O_4(OH)_4(BDC)_{5.76}(FE)_{0.48}$
UiO-66-AA	$Zr_6O_{4.91}(OH)_{3.09}(BDC)_{5.38}(AE)_{0.30}(FE)_{0.04}$	$Zr_6O_4(OH)_4(BDC)_{5.10}(AE)_{0.28}(FE)_{0.04}(H_2O/OH^-)_{1.47}$
UiO-66-BA	$Zr_6O_{1.29}(OH)_{6.71}(BDC)_{5.74}(BE)_{3.16}(FE)_{0.07}$	$Zr_6O_4(OH)_4(BDC)_{3.44}(BE)_{1.87}(FE)_{0.04}(H_2O/OH^-)_{3.18}$
UiO-67-FA	$Zr_6O_{4.84}(OH)_{3.16}(BPDC)_{5.52}(FE)_{0.13}$	$Zr_6O_4(OH)_4(BPDC)_{5.33}(FE)_{0.13}(H_2O/OH^-)_{1.22}$
UiO-67-AA	$Zr_6O_{4.46}(OH)_{3.54}(BPDC)_{5.68}(AE)_{0.16}(FE)_{0.02}$	$Zr_6O_4(OH)_4(BPDC)_{5.57}(AE)_{0.16}(FE)_{0.02}(H_2O/OH^-)_{0.68}$
UiO-67-BIPY-BA	$Zr_6O_{4.19}(OH)_{3.81}(BPDC)_{5.09}(BIPY)_{0.53}(BE)_{0.49}(FE)_{0.09}$	$Zr_6O_4(OH)_4(BPDC)_{4.70}(BIPY)_{0.48}(BE)_{0.46}(FE)_{0.08}(H_2O/OH^-)_{1.09}$
UiO-67-NH_2−BA	$Zr_6O_{3.50}(OH)_{4.50}(BPDC)_{4.89}(BPDC\text{-}NH_2)_{0.88}(BE)_{0.42}(FE)_{0.54}$	$Zr_6O_4(OH)_4(BPDC)_{4.52}(BPDC\text{-}NH2)_{0.81}(BE)_{0.38}(FE)_{0.51}(H_2O/OH^-)_{0.45}$

[a]Formate (FE), acetate (AE), and benzoate (BE).

nonmultivariate MOFs will be referred to as UiO-x-y, where x is either 66 or 67 and y is FA, AA, or BA depending on whether formic acid, acetic acid, or benzoic acid was used as the modulator, respectively. These materials have been characterized by powder X-ray diffraction (PXRD), TGA, liquid state NMR, energy dispersive X-ray (EDX) spectroscopy, and nitrogen adsorption measurements.

Synthesis of UiO-66. The UiO-66 samples were synthesized using an already reported procedure.[32] $ZrCl_4$ (0.24 g, 1 eqv.) and benzoic acid (1.88 g, 13 eqv.), acetic acid (1.0 mL, 17 eqv.), or formic acid (0.6 mL, 16 eqv.) were mixed in *N*,*N*-dimethylformamide (DMF) (40 mL, 500 eqv.) followed by addition of 1,4-benzenedicarboxylic acid (0.17 g, 1 eqv.). The solution was heated for 24 h at 120 °C with magnetic stirring before finally being filtrated twice with 20 mL of hot DMF and three times with 20 mL of acetone. To remove any residual solvents, the UiO-66 samples were filtrated continuously overnight using a Soxhlet extractor filled with acetone.

Synthesis of UiO-67. $ZrCl_4$ (0.24 g, 1 eqv.) and acetic acid (1.0 mL, 17 eqv.) or formic acid (0.6 mL, 16 eqv.) were mixed in DMF (40 mL, 500 eqv.) followed by the addition of 4,4′-biphenyldicarboxylic acid (0.25 g, 1 eqv.). The synthesis container was submerged in an oil bath at 120 °C under reflux. After 24 h the material was filtrated twice with 20 mL of hot DMF and three times with 20 mL of acetone.

Two multivariate UiO-67 samples have been synthesized using benzoic acid as the modulator. The first MOF was commercially purchased by PROFMOF A/S and was synthesized using 10% 2,2′-bipyridine-5,5′-dicarboxylic acid, denoted UiO-67-BIPY-BA. The second multivariate UiO-67 sample was synthesized using an already published procedure[33] and contains 20% 2,2′-diamino-[1,1′-biphenyl]-4,4′-dicarboxylic acid and is denoted UiO-67-NH_2−BA.

Detailed synthesis procedures are provided in Supporting Information, Section 2.

Powder X-ray Diffraction. A Bruker D8-A25 with a Lynxeye detector was used to obtain the PXRD results. A Ge (111) Johanssen monochromator was used to select Cu K-alpha-1 radiation. Measurements were performed from 2θ = 2−50 with a step size and speed of 0.019° and 0.1 s, respectively.

Thermogravimetric Analysis. TGA results were obtained on a Netzsch STA 449 F3 Jupiter instrument. The samples were heated to 800 °C using a heating rate of 5 °C/min in an Al_2O_3 crucible under a flow of 100 mL/min of synthetic air.

^{1}H Nuclear Magnetic Resonance. The NMR spectra were obtained using a Bruker AVIII HD 400 instrument equipped with a BACS-60 auto sampler. To dissolve the samples, a spatula tip of UiO-66/67 and 1 mL of a 0.1 M NaOD in D_2O solution was added to the centrifugation tube. After 15 min on a shaker, the sample was centrifuged and transferred to a sample holder. Other methods for digestion of Zr-based MOFs may also be applied (see refs 34−36 and refs therein).

Energy Dispersive X-ray Spectroscopy. EDX results were obtained using a Hitachi SU8230 Field Emission Electron Microscope. The acceleration voltage and ion current used are given for each figure summarizing the results.

Nitrogen Adsorption. Nitrogen adsorption isotherms were measured at −196 °C using a BelSorp mini II instrument after sample activation at 200 °C for 3 h using a Belprep vac II instrument. Surface areas were determined using the Brunauer−Emmett−Teller theory.

https://doi.org/10.1021/acs.chemmater.2c03744
Chem. Mater. 2023, 35, 3793−3800

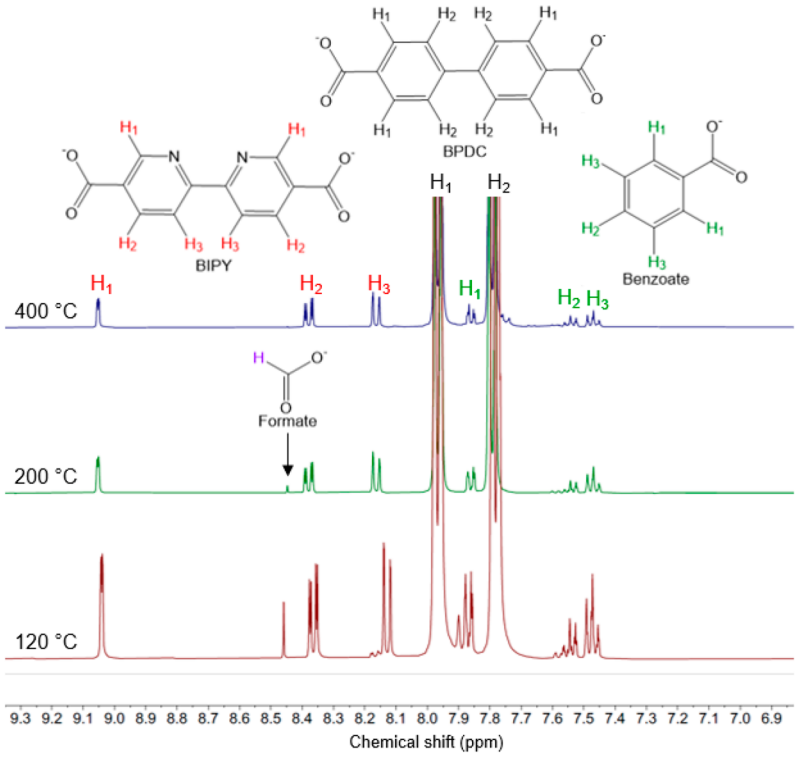

Figure 4. ^{1}H NMR spectrum (0.1 M NaOD in D_2O) of digested UiO-67-BIPY-BA. Red spectrum (bottom): sample was activated at 120 °C overnight; green spectrum (middle): sample was activated at 200 °C for 2 h; blue spectrum (top): sample was activated at 400 °C for 2 h.

PROCEDURE

The starting point for linker defect quantification is the MOF structure, which consists of a positively charged node, $Zr_6O_4(OH)_4^{12+}$, as well as organic and inorganic counterions that balance the node charge. To calculate the missing linker content in a MOF, the molar mass of the material (M_{MOF}), the quantity of organic counterions (a_i), and the quantity of inorganic counterions (b_j) must be known.

The molar mass of the material (M_{MOF}) can be determined by using eq 2, where $m_{200°C}$ and $m_{800°C}$ are the masses of the MOF measured during the TGA experiment at 200 and 800 °C, respectively. M_{ZrO_2} is the molar mass of ZrO_2.

$$M_{MOF} = \frac{m_{200°C}}{m_{800°C}} \times 6M_{ZrO_2} \tag{2}$$

This formula assumes that the material is fully decomposed at 800 °C and that six moles of ZrO_2 are formed per mol of UiO-67 during the decomposition (eq 3):

$$Zr_6O_4(OH)_4(C_{14}H_8O_4)_6(s) + 87O_2(g) \rightarrow 84CO_2(g) + 26H_2O(g) + 6ZrO_2(s) \tag{3}$$

The quantity of organic counterions (a_i) is determined by the ^{1}H NMR spectrum of the digested material and eq 4. In eq 4, A_i is the area of the peak corresponding to counterion i and H_i is the quantity of hydrogen atoms contributing to that specific peak. The values of a_i are arbitrarily determined by the relative areas of the peaks in the ^{1}H NMR spectrum and must be scaled to Zr (see below).

$$a_i = \frac{A_i}{H_i} \tag{4}$$

The quantity of inorganic counterions (b_j) is determined using eq 5 and EDX analysis. Here $\frac{B_j}{B_{Zr}}$ is the atomic % ratio of species j and zirconium obtained by EDX, which is multiplied by 6 because each SBU contains 6 Zr atoms.

$$b_j = 6 \times \frac{B_j}{B_{Zr}} \tag{5}$$

Finally, we know that the molar mass of the MOF must be the sum of all MOF components (i.e., the molar mass of the cluster and counterions) as shown in eq 6. The only unknowns of this equation are α, which is a scaling factor for the ratios of the organic counterions determined by ^{1}H NMR versus Zr_6, and β, which is the amount of H_2O/OH^- pairs acting as counterions. In addition, α and β can be correlated by using eq 7, which assumes that the global charge of the nodes (+12 e) must be compensated by −12 e charges from the counterions. Equation 7 was multiplied by −1 for clarity. The solution for α and β is shown in the Supporting Material, Section 1.2.

$$M_{MOF} = M_{Cluster} + \alpha \sum_1^i a_i \times M_i + \sum_1^j b_j \times M_j + \beta \times M_{OH^-} \tag{6}$$

$$12 = \alpha \sum_1^i -q_i \times a_i + \sum_1^j -q_j \times b_j + \beta \tag{7}$$

This methodology to compute missing linker defects is based on the following assumptions:

(1) **The decomposition product of the MOF is known.** The MOF decomposition reaction is important for calculating the molar mass of the material. This reaction

https://doi.org/10.1021/acs.chemmater.2c03744
Chem. Mater. 2023, 35, 3793−3800

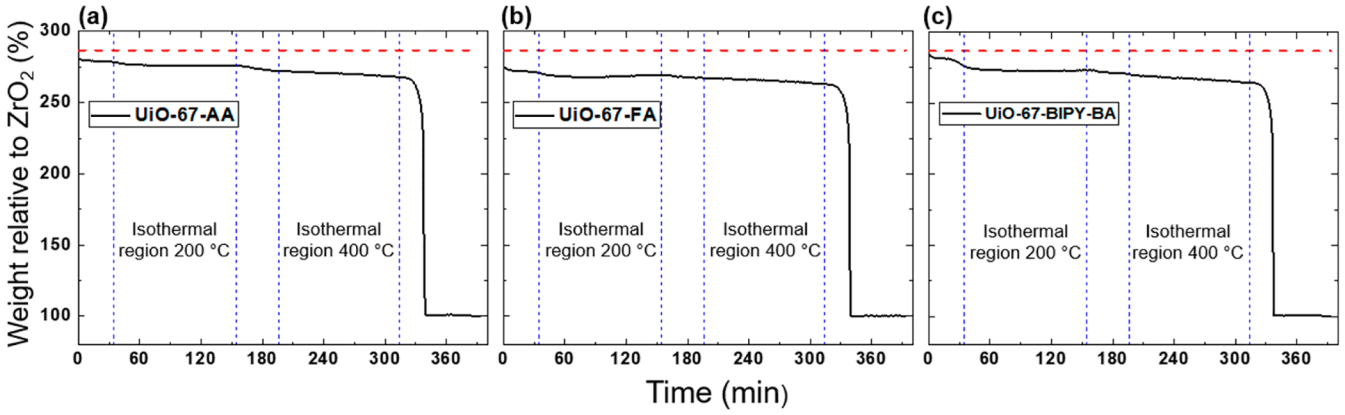

Figure 5. (a) TGA results for UiO-67-AA, (b) UiO-67-FA, and (c) UiO-67-BIPY-BA. The samples were heated from 30−800 °C with two isothermal regions which were kept for 2 h at 200 and 400 °C. The red dashed line indicates the theoretical mass of ideal and hydrated UiO-67 (286.8%).

for UiO-67 is given in eq 3 with CO_2, H_2O, and ZrO_2 as the main products. Other carbon containing products have been reported,[37] but the zirconium product is always ZrO_{2-x}. Our assumption becomes increasingly worse as x increases but x is typically quite small.[38] The oxygen deficiency, x, can be estimated after a TGA measurement by increasing the oxygen content and assuming that the change in mass originate from the incorporation of oxygen.[39]

(2) **No missing cluster defects are present in the material.** The presence of missing cluster defects is problematic as it will affect the decomposition reaction. Unfortunately, there is no accurate method to quantify missing cluster defects, although they can be detected by forbidden reflections in the X-ray diffractograms[29] or increased uptake of N_2 in the N_2 adsorption isotherm.[25]

(3) **The pores of the material are empty or contain species that can be quantified at 200 °C.** This assumption is important as any unknown species still present after activation at 200 °C will cause an overestimation in the molar mass of the material and will make the material appear less defective. This source of error is reduced by a thorough washing procedure and drying in air at 120 °C, after synthesis. In case the amounts of species in the pore are known, the formulas must be altered to accommodate the extra mass. A relevant example is the presence of DMF in UiO-66, where even extensive washing may not be enough to remove it from the pores. Fortunately, DMF is detectable as dimethylamine (DMA) using ^{1}H NMR and can easily be accounted for by adding a term in eq 6.[10]

(4) **The composition of the nodes at 200 °C is known.** As the **M-200** method determines the molar mass of the material at 200 °C, one must assume that the composition of the node is known at this temperature. For many MOFs the composition of the node is static and therefore one does not have to consider any change in mass due to change in the node. For the zirconium node, this is not the case as the node undergoes dehydration upon activation. Based on Shearer et al.'s previous work on UiO-66/67 MOFs, it is likely that the dehydration of these systems occurs between 250−350 °C.[29] Therefore, it is assumed that the composition of the nodes in the absence of counterions at 200 °C is $Zr_6O_4(OH)_4^{12+}$.

CHARACTERIZATION AND DISCUSSION

XRD, N_2 adsorption, NMR, TGA, and EDX data for the samples presented in this work are shown in Figures 4 and 5 and in Supporting Information, Figures S2−S14 and Tables S1−S6.

Thermal Stability of Counterions. To calculate the chemical composition of MOFs, the counterions must be identified and quantified at the reference conditions (see eqs 6 and 7). The UiO-66/67 samples were pretreated at three different temperatures, 120 °C overnight and 200 and 400 °C for 2 h. To determine the composition of the activated material, each sample was characterized by ^{1}H NMR (Figures 4 and S6−S11, Tables S1−S4), and the results are summarized in Tables S3 and S4. For both UiO-67-AA (Table S4) and UiO-67-FA (Table S4), no significant change in composition is observed after activation at 120 and 200 °C. The ^{1}H NMR spectrum for UiO-67-BIPY-BA (Table S4, Figure 4) suggests that some of the benzoate and formate is removed after activation at 200 °C; this is likely due to residual benzoate and DMF inside the pores of the material. This is further supported by the TGA curves for the UiO-67 materials where the plateau in the isothermal region of 200 °C is flat after an initial period of 5 min (Figure 5). When comparing the ratios of the organic species after activation at 200 and 400 °C, all the formate and acetate are removed for the UiO-67 samples, and for UiO-67-AA and UiO-67-FA the mass loss in the isothermal region of 400 °C is roughly 4.3% which is slightly lower than the expected mass loss caused by the dehydration of the node. For UiO-67-BIPY-BA, only 1/3 of the benzoate has been removed after heat treatment at 400 °C. The loss of benzoate is also indicated by the TGA results, where the mass is continuously decreasing in the isothermal region. The mass loss of the sample in this region is 6.1%, more than expected by the dehydration of the node (Figure 5c). For the UiO-67-NH_2-BA sample all the benzoate counterions and 2/3 of the BPDC-NH_2 linker have decomposed (Table S4), suggesting a severe decomposition of the material. For materials to be applicable for the **M-400** method, all counterions except for the linker must be removed before 400 °C; for samples containing only acetate and formate, the assumption made in the **M-400**

https://doi.org/10.1021/acs.chemmater.2c03744
Chem. Mater. 2023, 35, 3793−3800

method is valid, but this is not the case for the benzoate. Even for the UiO-67-BIPY-BA material, the BPDC:BIPY ratio changes slightly. This indicates that at 400 °C either BIPY or both BIPY and BPDC start decomposing, and therefore the **M-400** method is not suitable for MTV-MOFs either. The same trends were observed for the UiO-66 analogues (Table S3, Figures S6−S8) (*vide infra*).

Proof of Concept. The calculated chemical compositions of the seven samples presented in this work are summarized in Table 1 using both the **M-200** and the **M-400** methods. Comparing the compositions determined by the two methods, the **M-400** method is in most cases overestimating the quantity of counterions. This can be explained by the fact that charge compensation for the **M-400** method is achieved by altering the ratio of μ_3-O to μ_3-OH groups instead of introducing the H_2O/OH^- pair as the counterion. The overestimation of counterions using the **M-400** method is due to the larger mass of the H_2O/OH^- pair compared to the removal or addition of a single proton. This is the case for all the experimental samples presented in Table 1. The amounts of C, N, O, and Zr (in %) for UiO-67-FA, UiO-67-AA, and UiO-67-BIPY-BA determined by EDX and calculated using the **M-200** and **M-400** methods are summarized in Table S6. The calculated atomic percentage of carbon using the **M-400** method is larger than by using the **M-200** method as discussed above. Comparing these results to the atomic percentage of the carbon determined by EDX, the **M-200** method fits well for both UiO-67-FA and UiO-67-AA. The **M-200** method slightly overestimates the value for the UiO-67-BIPY-BA sample (65.8% versus 63.6% ± 2%). The **M-400** method overestimates the carbon percentage for both UiO-67-FA and UiO-67-BIPY-BA. The UiO-67-AA sample has fewer missing linker defects than both the formate and the benzoate analogue, and the **M-400** method is therefore able to accurately estimate the percentage of carbon.

The **M-400** method is especially unsuited for calculating missing linker defects in MOFs when benzoate is present as a counterion. This is because the assumption that all the monocarboxylate groups have been removed at 400 °C is not valid (Tables S3 and S4). The result is an inherent overestimation in both the linker quantity as well as the other counterions. This is further supported when comparing the results of the two methods for UiO-66/67-BA samples (Table 1). For UiO-67-BIPY-BA the **M-400** method leads to an overestimation of 0.39 linkers per node, while for UiO-66-BA, the method leads to an unphysical chemical formula where each cluster is coordinated to more than 12 species. As the **M-200** method evaluates the molar mass of the MOF at 200 °C, using both NMR and TGA combined, the method does not overestimate the quantity of counterions.

In some cases, the **M-400** method may underestimate the quantity of counterions. This occurs only when there are very few H_2O/OH^- counterions in the material and all the monocarboxylates have been removed at 400 °C.

These results highlight the importance of using both TGA and NMR when calculating the chemical composition of MOFs. TGA can be used to determine the molar mass of the material using eq 2, but it does not provide insight into the identity of the counterions present in the material. A crucial advantage of using both TGA and NMR simultaneously is the possibility to calculate the quantity of H_2O/OH^- pairs, which cannot be achieved by one single technique.

Returning finally to the assumptions that form the basis of the M-200 method, assumptions 3 and 4 were already accounted for in the Procedure section. Assumption 1, the assumed negligible fraction of oxygen vacancies in the end-product of TGA, ZrO_2, was verified by increasing the oxygen content of the gas feed at the end of the TGA measurement of UiO-67-BIPY-BA. No change in the final mass was observed, confirming the quantity of oxygen vacancies is negligible (see Figure S14). Assumption 2, no missing cluster defects being present in the material, was assessed by first noting that the pK_a values of all modulators used in this study (4.76, 4.19, and 3.77 for acetic acid, benzoic acid, and formic acid, respectively) were higher, and their concentration (≤17 eqv.) lower, than the critical values reported by Shearer et al. (pK_a < 3.77 and concentrations > 18 eqv., respectively).[27]

Moreover, inspection of the diffractograms for the samples did not reveal forbidden reflections at low 2theta values. The theoretical specific surface areas of UiO-66 and UiO-67 are 1187 $m^2\ g^{-1}$ and 3000 $m^2\ g^{-1}$, respectively, in good agreement with the measured values of samples presented herein (see Figures S4 and S5).[23] Overall, the investigations suggest few to no missing cluster defects in the studied materials.

CONCLUSION

In this work we have developed a new method for calculating missing linker defects in UiO type MOFs. We have showed that the **M-400** method does not provide satisfying results for MOFs containing temperature resistant counterions, such as benzoate and different linkers (MTV-MOFs). The new method, **M-200**, uses both TGA and NMR when calculating the chemical composition of the materials, which provide satisfying results for both the UiO-66 and UiO-67 samples. For the UiO-67-BIPY-BA sample it has been shown that the **M-400** method may overestimate the quantity of counterions whereas the **M-200** method is able to accurately determine the chemical composition. This highlights the importance of applying both TGA and NMR results together when calculating the chemical formulas of MOFs.

ASSOCIATED CONTENT

Supporting Information

The Supporting Information is available free of charge at https://pubs.acs.org/doi/10.1021/acs.chemmater.2c03744.

Detailed experimental procedures, detailed descriptions of the two methods (M-200 and M-400), and characterization (PXRD, nitrogen adsorption isotherms, ^{1}H NMR, TGA, and EDX) (PDF)

Excel file showcasing the use of the M-200 method (XLSX)

AUTHOR INFORMATION

Corresponding Author

Unni Olsbye − *SMN Centre for Material Science and Nanotechnology, Department of Chemistry, University of Oslo, N-0315 Oslo, Norway*; orcid.org/0000-0003-3693-2857; Email: unni.olsbye@kjemi.uio.no

Authors

Dag Kristian Sannes − *SMN Centre for Material Science and Nanotechnology, Department of Chemistry, University of Oslo, N-0315 Oslo, Norway*

Sigurd Øien-Ødegaard − *SMN Centre for Material Science and Nanotechnology, Department of Chemistry, University of Oslo, N-0315 Oslo, Norway*

Erlend Aunan − *SMN Centre for Material Science and Nanotechnology, Department of Chemistry, University of Oslo, N-0315 Oslo, Norway;* orcid.org/0000-0002-0589-7991

Ainara Nova − *SMN Centre for Material Science and Nanotechnology, Department of Chemistry and Hylleraas Centre for Quantum Molecular Sciences, Department of Chemistry, University of Oslo, N-0315 Oslo, Norway;* orcid.org/0000-0003-3368-7702

Complete contact information is available at: https://pubs.acs.org/10.1021/acs.chemmater.2c03744

Notes

The authors declare no competing financial interest.

■ ACKNOWLEDGMENTS

Isabelle Gerz is acknowledged for synthesis of UiO-67-NH_2-BA. D.S. and U.O. acknowledge the Research Council of Norway for financial support (Grant No. 288331 CO2LO). A.N. acknowledge the Research Council of Norway for financial support (Grant No. 314321 CO2pCat).

■ REFERENCES

(1) Zhu, Y.; Zheng, J.; Ye, J.; Cui, Y.; Koh, K.; Kovarik, L.; Camaioni, D. M.; Fulton, J. L.; Truhlar, D. G.; Neurock, M.; Cramer, C. J.; Gutiérrez, O. Y.; Lercher, J. A. Copper-zirconia interfaces in UiO-66 enable selective catalytic hydrogenation of CO2 to methanol. *Nat. Commun.* **2020**, *11* (1), 5849.

(2) An, B.; Zhang, J.; Cheng, K.; Ji, P.; Wang, C.; Lin, W. Confinement of Ultrasmall Cu/ZnOx Nanoparticles in Metal−Organic Frameworks for Selective Methanol Synthesis from Catalytic Hydrogenation of CO2. *J. Am. Chem. Soc.* **2017**, *139* (10), 3834−3840.

(3) Safaei, M.; Foroughi, M. M.; Ebrahimpoor, N.; Jahani, S.; Omidi, A.; Khatami, M. A review on metal-organic frameworks: Synthesis and applications. *TrAC Trends in Analytical Chemistry* **2019**, *118*, 401−425.

(4) Qian, Q.; Asinger, P. A.; Lee, M. J.; Han, G.; Mizrahi Rodriguez, K.; Lin, S.; Benedetti, F. M.; Wu, A. X.; Chi, W. S.; Smith, Z. P. MOF-Based Membranes for Gas Separations. *Chem. Rev.* **2020**, *120* (16), 8161−8266.

(5) Bai, Y.; Dou, Y.; Xie, L.-H.; Rutledge, W.; Li, J.-R.; Zhou, H.-C. Zr-based metal−organic frameworks: design, synthesis, structure, and applications. *Chem. Soc. Rev.* **2016**, *45* (8), 2327−2367.

(6) Zhao, S.; Tan, C.; He, C.-T.; An, P.; Xie, F.; Jiang, S.; Zhu, Y.; Wu, K.-H.; Zhang, B.; Li, H.; Zhang, J.; Chen, Y.; Liu, S.; Dong, J.; Tang, Z. Structural transformation of highly active metal−organic framework electrocatalysts during the oxygen evolution reaction. *Nature Energy* **2020**, *5* (11), 881−890.

(7) Wißmann, G.; Schaate, A.; Lilienthal, S.; Bremer, I.; Schneider, A. M.; Behrens, P. Modulated synthesis of Zr-fumarate MOF. *Microporous Mesoporous Mater.* **2012**, *152*, 64−70.

(8) He, X.; Liao, Y.; Tan, J.; Li, G.; Yin, F. Defective UiO-66 toward boosted electrochemical nitrogen reduction to ammonia. *Electrochim. Acta* **2022**, *409*, 139988.

(9) Han, Y.; Liu, M.; Li, K.; Zuo, Y.; Wei, Y.; Xu, S.; Zhang, G.; Song, C.; Zhang, Z.; Guo, X. Facile synthesis of morphology and size-controlled zirconium metal−organic framework UiO-66: the role of hydrofluoric acid in crystallization. *CrystEngComm* **2015**, *17* (33), 6434−6440.

(10) Shearer, G. C.; Chavan, S.; Ethiraj, J.; Vitillo, J. G.; Svelle, S.; Olsbye, U.; Lamberti, C.; Bordiga, S.; Lillerud, K. P. Tuned to Perfection: Ironing Out the Defects in Metal−Organic Framework UiO-66. *Chem. Mater.* **2014**, *26* (14), 4068−4071.

(11) Kirchon, A.; Feng, L.; Drake, H. F.; Joseph, E. A.; Zhou, H.-C. From fundamentals to applications: a toolbox for robust and multifunctional MOF materials. *Chem. Soc. Rev.* **2018**, *47* (23), 8611−8638.

(12) Schaate, A.; Roy, P.; Godt, A.; Lippke, J.; Waltz, F.; Wiebcke, M.; Behrens, P. Modulated Synthesis of Zr-Based Metal−Organic Frameworks: From Nano to Single Crystals. *Chemistry − A European Journal* **2011**, *17* (24), 6643−6651.

(13) Moosavi, S. M.; Nandy, A.; Jablonka, K. M.; Ongari, D.; Janet, J. P.; Boyd, P. G.; Lee, Y.; Smit, B.; Kulik, H. J. Understanding the diversity of the metal-organic framework ecosystem. *Nat. Commun.* **2020**, *11* (1), 4068.

(14) Winarta, J.; Shan, B.; McIntyre, S. M.; Ye, L.; Wang, C.; Liu, J.; Mu, B. A Decade of UiO-66 Research: A Historic Review of Dynamic Structure, Synthesis Mechanisms, and Characterization Techniques of an Archetypal Metal−Organic Framework. *Cryst. Growth Des.* **2020**, *20* (2), 1347−1362.

(15) Athar, M.; Rzepka, P.; Thoeny, D.; Ranocchiari, M.; Anton van Bokhoven, J. Thermal degradation of defective high-surface-area UiO-66 in different gaseous environments. *RSC Adv.* **2021**, *11* (61), 38849−38855.

(16) Wu, H.; Yildirim, T.; Zhou, W. Exceptional Mechanical Stability of Highly Porous Zirconium Metal−Organic Framework UiO-66 and Its Important Implications. *J. Phys. Chem. Lett.* **2013**, *4* (6), 925−930.

(17) Ahmadijokani, F.; Mohammadkhani, R.; Ahmadipouya, S.; Shokrgozar, A.; Rezakazemi, M.; Molavi, H.; Aminabhavi, T. M.; Arjmand, M. Superior chemical stability of UiO-66 metal-organic frameworks (MOFs) for selective dye adsorption. *Chemical Engineering Journal* **2020**, *399*, 125346.

(18) Valenzano, L.; Civalleri, B.; Chavan, S.; Bordiga, S.; Nilsen, M. H.; Jakobsen, S.; Lillerud, K. P.; Lamberti, C. Disclosing the Complex Structure of UiO-66 Metal Organic Framework: A Synergic Combination of Experiment and Theory. *Chem. Mater.* **2011**, *23* (7), 1700−1718.

(19) Lv, X.-L.; Yuan, S.; Xie, L.-H.; Darke, H. F.; Chen, Y.; He, T.; Dong, C.; Wang, B.; Zhang, Y.-Z.; Li, J.-R.; Zhou, H.-C. Ligand Rigidification for Enhancing the Stability of Metal−Organic Frameworks. *J. Am. Chem. Soc.* **2019**, *141* (26), 10283−10293.

(20) DeCoste, J. B.; Peterson, G. W.; Jasuja, H.; Glover, T. G.; Huang, Y.-g.; Walton, K. S. Stability and degradation mechanisms of metal−organic frameworks containing the Zr6O4(OH)4 secondary building unit. *Journal of Materials Chemistry A* **2013**, *1* (18), 5642−5650.

(21) Yuan, S.; Feng, L.; Wang, K.; Pang, J.; Bosch, M.; Lollar, C.; Sun, Y.; Qin, J.; Yang, X.; Zhang, P.; Wang, Q.; Zou, L.; Zhang, Y.; Zhang, L.; Fang, Y.; Li, J.; Zhou, H. C. Stable Metal-Organic Frameworks: Design, Synthesis, and Applications. *Adv. Mater.* **2018**, *30* (37), 1704303.

(22) Feng, D.; Wang, K.; Wei, Z.; Chen, Y.-P.; Simon, C. M.; Arvapally, R. K.; Martin, R. L.; Bosch, M.; Liu, T.-F.; Fordham, S.; Yuan, D.; Omary, M. A.; Haranczyk, M.; Smit, B.; Zhou, H.-C. Kinetically tuned dimensional augmentation as a versatile synthetic route towards robust metal−organic frameworks. *Nat. Commun.* **2014**, *5* (1), 5723.

(23) Cavka, J. H.; Jakobsen, S.; Olsbye, U.; Guillou, N.; Lamberti, C.; Bordiga, S.; Lillerud, K. P. A New Zirconium Inorganic Building Brick Forming Metal Organic Frameworks with Exceptional Stability. *J. Am. Chem. Soc.* **2008**, *130* (42), 13850−13851.

(24) Wu, H.; Chua, Y. S.; Krungleviciute, V.; Tyagi, M.; Chen, P.; Yildirim, T.; Zhou, W. Unusual and highly tunable missing-linker defects in zirconium metal-organic framework UiO-66 and their important effects on gas adsorption. *J. Am. Chem. Soc.* **2013**, *135* (28), 10525−32.

(25) Cliffe, M. J.; Wan, W.; Zou, X.; Chater, P. A.; Kleppe, A. K.; Tucker, M. G.; Wilhelm, H.; Funnell, N. P.; Coudert, F.-X.; Goodwin,

A. L. Correlated defect nanoregions in a metal−organic framework. *Nat. Commun.* **2014**, *5* (1), 4176.
(26) Wang, J.; Liu, L.; Chen, C.; Dong, X.; Wang, Q.; Alfilfil, L.; AlAlouni, M. R.; Yao, K.; Huang, J.; Zhang, D.; Han, Y. Engineering effective structural defects of metal−organic frameworks to enhance their catalytic performances. *Journal of Materials Chemistry A* **2020**, *8* (8), 4464−4472.
(27) Shearer, G. C.; Chavan, S.; Bordiga, S.; Svelle, S.; Olsbye, U.; Lillerud, K. P. Defect Engineering: Tuning the Porosity and Composition of the Metal−Organic Framework UiO-66 via Modulated Synthesis. *Chem. Mater.* **2016**, *28* (11), 3749−3761.
(28) Van de Voorde, B.; Stassen, I.; Bueken, B.; Vermoortele, F.; De Vos, D.; Ameloot, R.; Tan, J.-C.; Bennett, T. D. Improving the mechanical stability of zirconium-based metal−organic frameworks by incorporation of acidic modulators. *Journal of Materials Chemistry A* **2015**, *3* (4), 1737−1742.
(29) Shearer, G. C.; Vitillo, J. G.; Bordiga, S.; Svelle, S.; Olsbye, U.; Lillerud, K. P. Functionalizing the Defects: Postsynthetic Ligand Exchange in the Metal Organic Framework UiO-66. *Chem. Mater.* **2016**, *28* (20), 7190−7193.
(30) Trickett, C. A.; Gagnon, K. J.; Lee, S.; Gándara, F.; Bürgi, H.-B.; Yaghi, O. M. Definitive Molecular Level Characterization of Defects in UiO-66 Crystals. *Angew. Chem., Int. Ed.* **2015**, *54* (38), 11162−11167.
(31) Øien, S.; Wragg, D.; Reinsch, H.; Svelle, S.; Bordiga, S.; Lamberti, C.; Lillerud, K. P. Detailed Structure Analysis of Atomic Positions and Defects in Zirconium Metal−Organic Frameworks. *Cryst. Growth Des.* **2014**, *14* (11), 5370−5372.
(32) Wei, R.; Gaggioli, C. A.; Li, G.; Islamoglu, T.; Zhang, Z.; Yu, P.; Farha, O. K.; Cramer, C. J.; Gagliardi, L.; Yang, D.; Gates, B. C. Tuning the Properties of Zr6O8 Nodes in the Metal Organic Framework UiO-66 by Selection of Node-Bound Ligands and Linkers. *Chem. Mater.* **2019**, *31* (5), 1655−1663.
(33) Gerz, I.; Jannuzzi, S. A. V.; Hylland, K. T.; Negri, C.; Wragg, D. S.; Øien-Ødegaard, S.; Tilset, M.; Olsbye, U.; DeBeer, S.; Amedjkouh, M. Structural Elucidation, Aggregation, and Dynamic Behaviour of N,N,N,N-Copper(I) Schiff Base Complexes in Solid and in Solution: A Combined NMR, X-ray Spectroscopic and Crystallographic Investigation. *Eur. J. Inorg. Chem.* **2021**, *2021* (46), 4762−4775.
(34) Yuan, Y.; Yu, J.; Chen, H.; Bang, K.-T.; Pan, D.; Kim, Y. Thiol-functionalized Zr metal-organic frameworks for efficient removal of Fe3+ from water. *Cell Reports Physical Science* **2022**, *3* (3), 100783.
(35) Bohigues, B.; Rojas-Buzo, S.; Moliner, M.; Corma, A. Coordinatively Unsaturated Hf-MOF-808 Prepared via Hydrothermal Synthesis as a Bifunctional Catalyst for the Tandem N-Alkylation of Amines with Benzyl Alcohol. *ACS Sustainable Chem. Eng.* **2021**, *9* (47), 15793−15806.
(36) Howarth, A. J.; Peters, A. W.; Vermeulen, N. A.; Wang, T. C.; Hupp, J. T.; Farha, O. K. Best Practices for the Synthesis, Activation, and Characterization of Metal−Organic Frameworks. *Chem. Mater.* **2017**, *29* (1), 26−39.
(37) Goodenough, I.; Devulapalli, V. S. D.; Xu, W.; Boyanich, M. C.; Luo, T.-Y.; De Souza, M.; Richard, M.; Rosi, N. L.; Borguet, E. Interplay between Intrinsic Thermal Stability and Expansion Properties of Functionalized UiO-67 Metal−Organic Frameworks. *Chem. Mater.* **2021**, *33* (3), 910−920.
(38) Imparato, C.; Fantauzzi, M.; Passiu, C.; Rea, I.; Ricca, C.; Aschauer, U.; Sannino, F.; D'Errico, G.; De Stefano, L.; Rossi, A.; Aronne, A. Unraveling the Charge State of Oxygen Vacancies in ZrO2−x on the Basis of Synergistic Computational and Experimental Evidence. *J. Phys. Chem. C* **2019**, *123* (18), 11581−11590.
(39) Matsushima, Y.; Kakinuma, N.; Takahashi, H.; Kondo, A.; Maeda, K.; Suzuki, T.; Kambe, S. Thermogravimetric investigation of oxygen deficiency in SnO2 reduced at 500°C or below. *Solid State Ionics* **2017**, *308*, 101−106.

https://doi.org/10.1021/acs.chemmater.2c03744
Chem. Mater. 2023, 35, 3793−3800